Paper accepted for presentation at 2009 IEEE Bucharest Power Tech Conference, June 28th - July 2nd, Bucharest, Romania

Steady-State Solution of a VFT Park Using the Limit Cycle Method and a Reduced Order Model

L. Contreras-Aguilar, *Student Member IEEE* and N. García, *Member IEEE*

***Abstract*—A VFT park model suitable for stability analyses of asynchronous links is presented in this work. This model allows the simulation of multi-unit VFTs operated in parallel in order to increase the power transfer between two electric power systems. The backbone of the VFT model relies on a reduced order model of a wound-rotor induction machine. The VFT control system includes power and speed regulators in order to provide a smooth dynamic operation. The computation of the steady-state operating point is achieved with the limit cycle method based on a Newton method and the Poincaré map. This approach is particularly useful for the fast determination of the steady-state operating point of the variable frequency transformer because of the inherently large inertia of its rotary machine, which may cause a prolonged transient response after a system disturbance. The computation of the steady-state operating point with an acceleration procedure based on the limit cycle method paves the way to carry-out efficient stability studies. The steady-state operating point of a VFT park consisting of three 100 MW VFT units is computed for different operating scenarios.**

***Index Terms*—Variable Frequency Transformer, Wound Rotor Induction Machine, Limit Cycle Method, Steady-State.**

I. List of Symbols

ψ	flux linkage	r_s	stator resistance
x_s	stator leakage reactance	r_r	rotor resistance
x_r	rotor leakage reactance	X_s	stator reactance
x_m	magnetizing reactance	X_r	rotor reactance
H	constant of inertia	θ_m	rotor position
T_m	mechanic torque	ω_m	rotor speed
D_m	damping coefficient	ω_s	stator frequency
e	synchronous reference frame	ω_r	rotor frequency
s	stator reference frame	ω_b	base frequency
r	rotor reference frame	i	VFT number
q	quadrature-axis quantity	d	direct-axis quantity
n	number of VFT in the park	C	capacitance
$\mathbf{\Phi}$	transition matrix	$\mathbf{I}$	identity matrix

II. Introduction

RECENT breakthroughs in power transmission technology have favoured the development of the Variable Frequency Transformer (VFT), which represents an attractive alternative to provide control of power transfer in both directions between two electric grids [1]. The backbone of this comprehensive power flow controller is essentially a Wound Rotor Induction Machine (WRIM), where one power grid is connected to the stator side and another power network is connected to the rotor side. The torque applied on the rotor's shaft provides power flow bidirectional control.

The development of state of the art VFT installations have received special attention in contributions based on power flow [1] and real-time simulations [2]. An EMTP-based approach is presented in [3] for a set of transient studies such as energization and faults, while real-time simulations tests under severe grid disturbances have been reported for the second VFT installation worldwide [4]-[5]. Furthermore, a new high power asynchronous link between Manitoba and Ontario is proposed in [6], where two technologies based on HVDC back-to-back converters and VFTs are analyzed for this potential project. On the other hand, there is an increasing interest to develop new projects using a set of VFTs operating in a coordinated fashion [7]. However, no contributions can be found in the open literature to describe the operation of a set of VFTs working together.

In this work, a VFT Park model described with a set of parallel VFT units is presented. Each one of the multiple VFTs connected in parallel is defined with a reduced order model and includes its transformers, capacitor banks and the control system. Two basic regulators for power and speed control are included in order to provide a mechanic torque drive. The steady-state operating point solution of a VFT park consisting of three parallel VFT units is computed with an acceleration procedure based on the limit cycle method.

III. VFT Park Model

Fig. 1 shows the configuration of the VFT park proposed in this work for power exchange between two asynchronous power grids. The VFT park consists of a set of n VFT units connected in parallel, where each unit is modelled with a WRIM, coupling transformers and capacitor banks. The VFT model is a fourth order model in which the state variables are the rotor flux linkage, the rotor speed and the rotor position. The control system consists of a power regulator working together with a speed regulator to adjust the mechanic torque drive.

A. VFT Reduced-Order Model

Assuming that the stator transient of the induction machine in the synchronous reference frame is neglected, the terms $d\psi/dt$ in the stator voltage equations can be discarded [8]. Then, the voltage equations are,

$$\begin{bmatrix}0\\0\end{bmatrix}=\begin{bmatrix}0 & -\omega_s^e/\omega_b\\ \omega_s^e/\omega_b & 0\end{bmatrix}\begin{bmatrix}\psi_{qs,i}^e\\ \psi_{ds,i}^e\end{bmatrix}-\begin{bmatrix}r_s & 0\\ 0 & r_s\end{bmatrix}\begin{bmatrix}i_{qs,i}^e\\ i_{ds,i}^e\end{bmatrix}+\begin{bmatrix}1 & 0\\ 0 & 1\end{bmatrix}\begin{bmatrix}v_{qs,i}\\ v_{ds,i}\end{bmatrix} \quad (1)$$

and the rotor voltage equations are defined as,

The authors are with the División de Estudios de Posgrado, Facultad de Ingeniería Eléctrica, Universidad Michoacana de San Nicolás de Hidalgo, Morelia, Michoacán, 58030, Mexico. (Phone/fax: +52-443-3279728; e-mail: luisc@ucol.mx; gbarriga@zeus.umich.mx)

978-1-4244-2235-7/09/$25.00 ©2009 IEEE

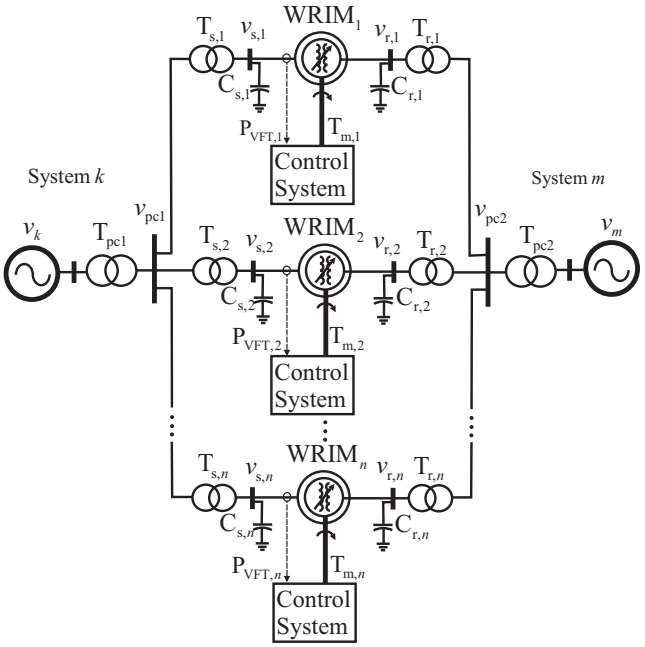

Fig. 1. VFT Park general configuration.

$$\frac{1}{\omega_b}\frac{d}{dt}\begin{bmatrix}\psi^e_{qr,i}\\ \psi^e_{dr,i}\end{bmatrix}=\begin{bmatrix}0 & -s_i\\ s_i & 0\end{bmatrix}\begin{bmatrix}\psi^e_{qr,i}\\ \psi^e_{dr,i}\end{bmatrix}-\begin{bmatrix}r_r & 0\\ 0 & r_r\end{bmatrix}\begin{bmatrix}i^e_{qr,i}\\ i^e_{dr,i}\end{bmatrix}+\begin{bmatrix}a & b\\ -b & a\end{bmatrix}\begin{bmatrix}v_{qr,i}\\ v_{dr,i}\end{bmatrix} \quad (2)$$

where $s_i=(\omega^e_s-\omega_{m,i})/\omega_b$, $\omega^e_s/\omega_b=1$ and the terms $a=\cos\theta_{m,i}$, $b=\sin\theta_{m,i}$ transform rotor voltages to the synchronous reference frame [8]. The subscript *i* indicates the VFT number (*i*=1…*n*).

Solving (1) for $\psi^e_{qs,i}$ and $\psi^e_{ds,i}$ results,

$$\begin{bmatrix}\psi^e_{qs,i}\\ \psi^e_{ds,i}\end{bmatrix}=\begin{bmatrix}-r_s & 0\\ 0 & r_s\end{bmatrix}\begin{bmatrix}i^e_{qs,i}\\ i^e_{ds,i}\end{bmatrix}+\begin{bmatrix}1 & 0\\ 0 & -1\end{bmatrix}\begin{bmatrix}v_{qs,i}\\ v_{ds,i}\end{bmatrix} \quad (3)$$

and substituting in the current equations for the WRIM,

$$\begin{bmatrix}i^e_{qs,i}\\ i^e_{ds,i}\\ i^e_{qr,i}\\ i^e_{dr,i}\end{bmatrix}=\frac{1}{X_{D,i}}\begin{bmatrix}X_{r,i} & 0 & -x_{m,i} & 0\\ 0 & X_{r,i} & 0 & -x_{m,i}\\ -x_{m,i} & 0 & X_{s,i} & 0\\ 0 & -x_{m,i} & 0 & X_{s,i}\end{bmatrix}\begin{bmatrix}\psi^e_{qs,i}\\ \psi^e_{ds,i}\\ \psi^e_{qr,i}\\ \psi^e_{dr,i}\end{bmatrix} \quad (4)$$

then the stator and rotor currents can be computed as,

$$\begin{bmatrix}i^e_{qs,i}\\ i^e_{ds,i}\\ i^e_{qr,i}\\ i^e_{dr,i}\end{bmatrix}=\begin{bmatrix}X_{D,i} & -r_{s,i}X_{r,i} & 0 & 0\\ r_{s,i}X_{r,i} & X_{D,i} & 0 & 0\\ 0 & r_{s,i}x_{m,i} & X_{D,i} & 0\\ -r_{s,i}x_{m,i} & 0 & 0 & X_{D,i}\end{bmatrix}^{-1}\begin{bmatrix}0 & -X_{r,i} & -x_{m,i} & 0\\ X_{r,i} & 0 & 0 & -x_{m,i}\\ 0 & x_{m,i} & X_{s,i} & 0\\ -x_{m,i} & 0 & 0 & X_{s,i}\end{bmatrix}\begin{bmatrix}v^e_{qs,i}\\ v^e_{ds,i}\\ \psi^e_{qr,i}\\ \psi^e_{dr,i}\end{bmatrix} \quad (5)$$

with $X_{s,i}=x_{s,i}+x_{m,i}$, $X_{r,i}=x_{r,i}+x_{m,i}$ and $X_{D,i}=X_{s,i}X_{r,i}-x^2_{m,i}$ [8].

The electromagnetic torque and mechanical equations are,

$$T_{e,i}=x_{m,i}(i^e_{qs,i}i^e_{dr,i}-i^e_{ds,i}i^e_{qr,i}) \quad (6)$$

$$\frac{d}{dt}\left[\frac{\omega_{m,i}}{\omega_b}\right]=\frac{T_{e,i}-T_{m,i}-D_{m,i}\omega_{m,i}}{2H_i} \quad (7)$$

$$\frac{d}{dt}\theta_{m,i}=\omega_b\left[\frac{\omega_{m,i}}{\omega_b}\right]-(\omega^e_s-\omega^e_r) \quad (8)$$

The transients associated with the remaining components of the VFT park can be neglected in order to obtain a set of algebraic equations. Hence, the transformers' currents on the stator and rotor side of each WRIM are,

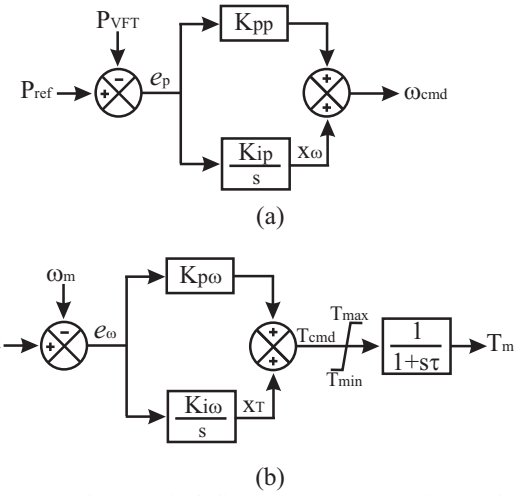

Fig. 2. VFT control system including (a).- a power regulator and (b).- a speed regulator.

$$\begin{bmatrix}i_{q,Tsi}\\ i_{d,Tsi}\end{bmatrix}=\begin{bmatrix}0 & \omega^e_s C_{si}\\ -\omega^e_s C_{si} & 0\end{bmatrix}\begin{bmatrix}v^e_{qs,i}\\ v^e_{ds,i}\end{bmatrix}+\begin{bmatrix}i^e_{qs,i}\\ i^e_{ds,i}\end{bmatrix} \quad (9)$$

$$\begin{bmatrix}i_{q,Tri}\\ i_{d,Tri}\end{bmatrix}=\begin{bmatrix}0 & \omega^e_r C_{ri}\\ -\omega^e_r C_{ri} & 0\end{bmatrix}\begin{bmatrix}v^e_{qr,i}\\ v^e_{dr,i}\end{bmatrix}+\begin{bmatrix}i^e_{qr,i}\\ i^e_{dr,i}\end{bmatrix} \quad (10)$$

The voltages at the points of common coupling can be expressed algebraically as,

$$\begin{bmatrix}v_{q,pc1}\\ v_{d,pc1}\end{bmatrix}=-\begin{bmatrix}r_{Tpc1} & x_{Tpc1}\\ -x_{Tpc1} & r_{Tpc1}\end{bmatrix}\begin{bmatrix}\sum_{i=1}^{n} i_{q,Tsi} & \sum_{i=1}^{n} i_{d,Tsi}\end{bmatrix}^T+\begin{bmatrix}v_{q,k}\\ v_{d,k}\end{bmatrix} \quad (11)$$

$$\begin{bmatrix}v_{q,pc2}\\ v_{d,pc2}\end{bmatrix}=-\begin{bmatrix}r_{Tpc2} & x_{Tpc2}\\ -x_{Tpc2} & r_{Tpc2}\end{bmatrix}\begin{bmatrix}\sum_{i=1}^{n} i_{q,Tri} & \sum_{i=1}^{n} i_{d,Tri}\end{bmatrix}^T+\begin{bmatrix}v_{q,m}\\ v_{d,m}\end{bmatrix} \quad (12)$$

The new values for voltages $v^e_{qd,s}$ and $v^e_{qd,r}$ at each WRIM to be used in the next integration step are calculated as,

$$\begin{bmatrix}v^e_{qs,i}\\ v^e_{ds,i}\end{bmatrix}=-\begin{bmatrix}r_{Tsi} & x_{Tsi}\\ -x_{Tsi} & r_{Tsi}\end{bmatrix}\begin{bmatrix}i_{q,Tsi}\\ i_{d,Tsi}\end{bmatrix}+\begin{bmatrix}v_{q,pc1}\\ v_{d,pc1}\end{bmatrix} \quad (13)$$

$$\begin{bmatrix}v_{qr,i}\\ v_{dr,i}\end{bmatrix}=-\begin{bmatrix}r_{Tri} & x_{Tri}\\ -x_{Tri} & r_{Tri}\end{bmatrix}\begin{bmatrix}i_{q,Tri}\\ i_{d,Tri}\end{bmatrix}+\begin{bmatrix}v_{q,pc2}\\ v_{d,pc2}\end{bmatrix} \quad (14)$$

B. Control System

Fig. 2 illustrates an elementary control system for the VFT, which provides power regulation by adjusting the rotor speed. The power regulator shown in Fig. 2(a) measures the power flow throughout the VFT and compares it with a reference power. The error signal is fed to a PI controller and its output represents a speed command (ω_{cmd}). This controller is defined as,

$$\frac{d}{dt}x_\omega=K_{ip}(P_{ref}-P_{VFT}) \quad (15)$$

and the speed command

$$\omega_{cmd}=x_\omega+K_{pp}(P_{ref}-P_{VFT}) \quad (16)$$

Fig. 2(b) shows the speed regulator block diagram, where the speed command ω_{cmd} determined by the power regulator is compared with the rotor speed ω_m. A PI controller determines the commanded torque T_{cmd} from the speed error signal. A

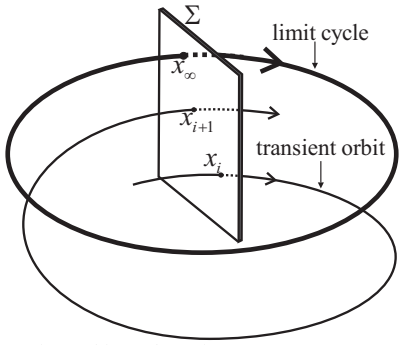

Fig. 3. Single transient orbit on the Poincaré map.

torque limiter prevents the torque command to be within the motor capability. In this work, the rate of change of the driving torque command is allowed to take values between ±5 pu. The torque drive feeds a first order system that represents the dynamic response of the drive motor. Then, the speed regulator is defined with two differential equations,

$$\frac{d}{dt}\begin{bmatrix} x_T \\ T_m \end{bmatrix} = \begin{bmatrix} 0 & 0 \\ \tau^{-1} & -\tau^{-1} \end{bmatrix}\begin{bmatrix} x_T \\ T_m \end{bmatrix} + \begin{bmatrix} K_{i\omega} & -K_{i\omega} \\ K_{p\omega}\tau^{-1} & -K_{p\omega}\tau^{-1} \end{bmatrix}\begin{bmatrix} \omega_{cmd} \\ \omega_m \end{bmatrix} \quad (17)$$

where

K_{pp} proportional gain of the power regulator,

K_{ip} integral gain of the power regulator,

$K_{p\omega}$ proportional gain of the speed regulator,

$K_{i\omega}$ integral gain of the speed regulator,

τ time constant of the drive motor.

IV. The Limit Cycle Method

An electric system can be described as,

$$\dot{\mathbf{x}} = f(t, \mathbf{x}), \quad \mathbf{x}(t_0) = \mathbf{x}_0 \quad (18)$$

where $\mathbf{x}$ is a m-dimensional state vector and $\mathbf{x}_0$ is the initial condition. If the set of Ordinary Differential Equations (ODEs) has a periodic driving force so that $f(t,\cdot)$ is also T-periodic, then it can be represented as a limit cycle for $\mathbf{x}_\infty$ in terms of another periodic element of $\mathbf{x}$ or in terms of an arbitrary T-periodical function [9].

Assuming a single transient orbit that starts at x_i and ends at x_{i+1} after one cycle of integration, its dynamic behavior is conveniently described by its intercepts on the Poincaré map Σ, (see Fig. 3). In the proximity of the limit cycle a Newton method can be used to determine the solution to the limit cycle. The transformation of the non-autonomous problem described in (18) into a variational problem has the form [10],

$$\Delta\dot{\mathbf{x}} = \mathbf{J}(t)\Delta\mathbf{x} \quad (19)$$

and the general solution matrix that calculates $\Delta\mathbf{x}$ is,

$$\Delta\mathbf{x}(T) = \mathbf{\Phi}(T)\Delta\mathbf{x}(0) \quad (20)$$

where $\mathbf{\Phi}$ and $\mathbf{J}$ are the transition and Jacobian matrix, respectively.

The solution of the state variables at the limit cycle is computed with a Newton method,

$$\mathbf{x}_\infty = \mathbf{x}_0 + (\mathbf{I} - \mathbf{\Phi})^{-1}(\mathbf{x}'_0 - \mathbf{x}_0) \quad (21)$$

where

$\mathbf{x}_\infty$ state variables at the limit cycle,

$\mathbf{x}_0$ state variables at the beginning of the base cycle,

$\mathbf{x}'_0$ state variables at the end of the base cycle.

A. Numerical Differentiation

The computation of the transition matrix $\mathbf{\Phi}$ can be performed with the use of a Numerical Differentiation (ND) procedure [10]. This process allows obtaining matrix $\mathbf{\Phi}$ by columns with a sequential perturbation of the state variables at the base cycle defined as,

$$\mathbf{x}_i = \mathbf{x}_0 + \xi e_i = \mathbf{x}_0 + \xi[0...1...0]_i^T \quad (22)$$

or

$$\mathbf{x}_i - \mathbf{x}_0 = \xi e_i \quad (23)$$

where ξ is a small value of 1×10^{-6} for $i = 1, 2, ..., m$.

From (20), the following relationship holds for a m-order problem,

$$\Delta\mathbf{x}_{i+1} = \mathbf{\Phi}\Delta\mathbf{x}_i \quad (24)$$

Substituting (23) in (24) results in the following relation,

$$\Delta\mathbf{x}_{i+1} = \mathbf{\Phi}\xi e_i \quad (25)$$

Therefore, matrix $\mathbf{\Phi}$ can be obtained from (25) as follows,

$$\mathbf{\Phi} = \frac{1}{\xi}\Delta\mathbf{x}_{i+1} \quad (26)$$

V. Asynchronous Link Test Case

The study case presented in this section consists of two asynchronous systems connected throughout a VFT park with three 100 MW VFT units. While the power system at the rotor side is 59 Hz, the power grid connected at the stator side has a frequency of 60 Hz. Both power networks maintain a phase angle difference of five degrees. Results are reported using the Runge-Kutta 4*th* order method and a 130 μs time step. The maximum mismatch is set to 1×10^{-8} in order to locate the steady-state operating point of the VFT park for its energization, a power transfer change and a fault clearing at VFT_2. The computational effort reported in this paper is measured in a PC dual core at 1.73 GHz and 1GB RAM memory. The VFT parameters used in this work are reported in the Appendix.

A. Dynamic Solution

In order to study the transient solution obtained with the proposed control system, a step power command and a power reversal are applied at t=0 and t=5 seconds, respectively. The power references for VFT_1, VFT_2 and VFT_3 are set to 0.7, 0.9 and 0.5 pu. Fig. 4(a) shows the mechanic torque drive provided by the speed driver, whilst Fig. 4(b) shows the active power flow response through the VFTs. Similar responses are reported in [1], where the transient settles down in approximately two seconds. On the other hand, Figs. 5 (a) and (b) show the total active and reactive power exchange throughout the VFT park when a three-phase fault takes place at VFT_2 on the rotor side. Comparative results are reported with the 4*th* order reduced model presented in this paper and a detailed model of order 6 described in [8]. As expected,

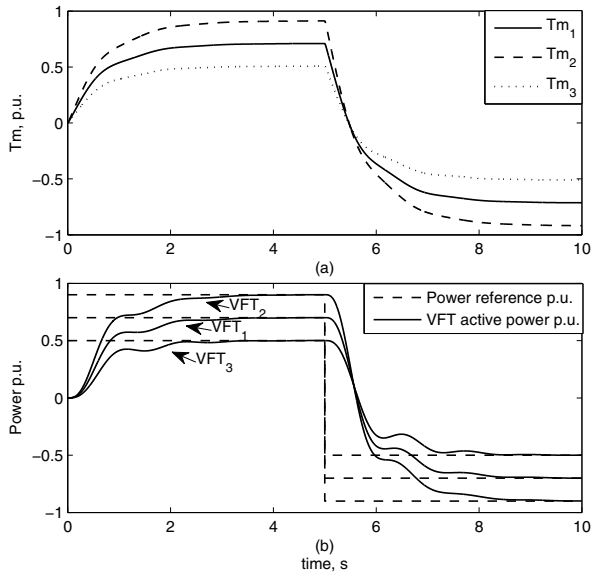

Fig.4. VFT responses to step power command for (a).- mechanic torque and (b).- active power flow.

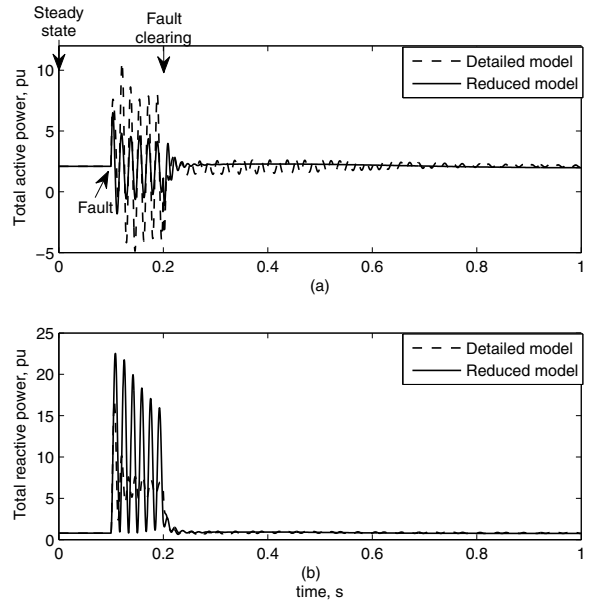

Fig. 5. Transient behavior during fault for (a).- total active power and (b).- total reactive power.

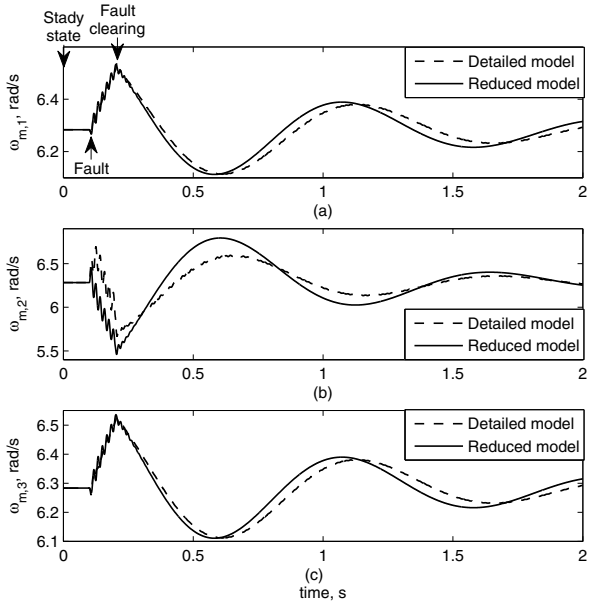

Fig. 6. Transient solution of rotor speed after fault clearing for (a).- $WRIM_1$, b).- $WRIM_2$ and c).- $WRIM_3$.

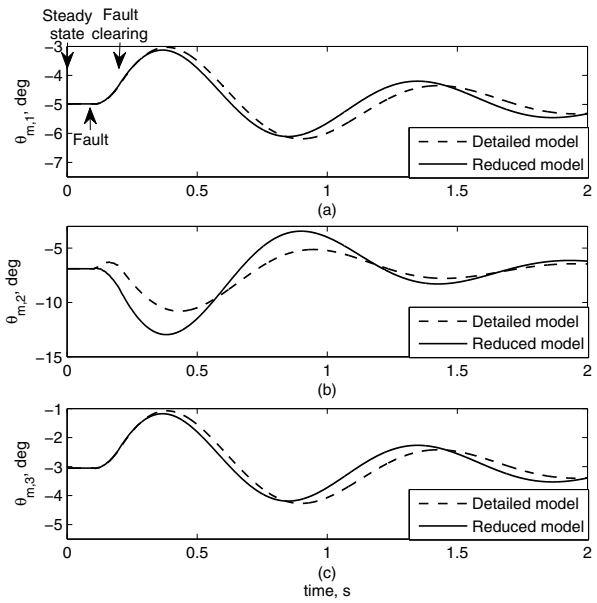

Fig. 7. Transient solution of rotor position after fault clearing for (a).- $WRIM_1$, (b).- $WRIM_2$ and (c).- $WRIM_3$.

discrepancies during transient are observed with the reduced model since the stator transient of WRIM has been neglected. However, no differences are observed at the steady-state operating point. Figs. 6 (a)-(c) and Figs. 7 (a)-(c) show the rotor speed and rotor position of $WRIM_{1,2,3}$, where it can be appreciated a transient solution during fault and a slow convergence to the steady-state after fault clearing.

B. Convergence to the Steady-State

Table I summarizes the maximum mismatches during convergence to the steady-state operating point using the limit cycle method. The first column indicates the number of applications (NA) of the Newton-Raphson method required to achieve the steady-state solution after computing a base cycle (BC), where five initial cycles of integration are run in order to determine the base cycle. It can be appreciated that 6 and 5 applications of the limit cycle method are required to reach the steady-state for the energization case with the detailed and reduced models, respectively. After the steady-state operating point is computed for the energization, the power transfer command is set to 0.7, 0.9 and 0.5 pu for VFT_1, VFT_2 and VFT_3, respectively, in order to increase the power transfer in the asynchronous link. A new base cycle is computed and only 5 applications of the limit cycle method are needed to find the steady-state operating point with both detailed and reduced models. Once the steady-state operating point for the power transfer scenario is computed, a three-phase fault is applied at the rotor side of the number two VFT unit. A new base cycle is determined after five cycles of integration and 5 and 4 applications of the limit cycle method are needed to find the steady-state operating point with the detailed and reduced models, respectively. It can be appreciated that the

TABLE I
ERRORS DURING CONVERGENCE TO THE STEADY-STATE OPERATING POINT

NA	Energization		Power Transfer		Fault in the WRIM$_5$	
	Detailed	Reduced	Detailed	Reduced	Detailed	Reduced
BC	1.9278e-2	5.7303e-2	4.4880e-2	4.4880e-2	1.3253e-2	1.8229e-2
1	3.9178e-3	5.2853e-3	3.2775e-3	1.3211e-2	1.4390e-3	1.1827e-3
2	7.7245e-5	1.5304e-4	3.7533e-5	1.7494e-4	1.3443e-5	2.1826e-5
3	9.0290e-6	4.6622e-6	3.7160e-7	1.7743e-6	6.6354e-7	1.1855e-7
4	2.4718e-7	9.9650e-8	4.8198e-8	4.1717e-8	1.7893e-8	5.33295-9
5	2.4467e-8	5.9402e-9	5.484e-10	1.4085e-9	7.569e-10	
6	5.064e-10					

computation of the steady-state operating point with the detailed model required more applications than the reduced model for the energization and fault scenario. Furthermore, speedup factors of 7.55, 3.96 and 10.12 are obtained with the application of the limit cycle method and the reduced order model for the energization, power transfer and fault test case, respectively. The speedup factor for each operating scenario is computed as,

$$S_{factor} = \frac{T_{BF\text{-}DM}}{T_{LCM\text{-}RM}} \tag{27}$$

where S_{factor} is the speedup factor $T_{BF\text{-}DM}$ is the elapsed time needed with the detailed model of order 6 and a Brute Force method, while $T_{LCM\text{-}RM}$ is the elapsed time required by the reduced model and the limit cycle method.

VI. CONCLUSIONS

A comprehensive VFT park model suitable for stability analyses has been presented in this paper. While a WRIM reduced order model allows the implementation of compact VFT models, the computation of the steady-state operating point with an acceleration procedure paves the way to carry-out efficient stability studies. The VFT control system incorporates power and speed regulators in order to provide a mechanic torque drive. As expected, discrepancies during the transient response using a detailed and reduced model have been reported. However, excellent agreement is observed with both models for the steady-state solution. Speedup factors of nearly 10 have been measured for the computation of the steady-state using reduced order models and the limit cycle method.

VII. APPENDIX

The VFT parameters [2] and the control system parameters used in this work are shown in Table II. The control system parameters were obtained by tuning the PI controller using the Ziegler-Nichol's method based on the response to a step command [11]. The additional parameters used in this paper are:

$r_{s,i} = 0.002$ $\quad r_{r,i} = 0.002$
$r_{Ts,i} = 0.009$ $\quad r_{Tr,i} = 0.009$
$x_{Tpc1} = 0.008$ $\quad x_{Tpc2} = 0.008$
$r_{Tpc1} = 0.0089$ $\quad r_{Tpc2} = 0.0089$
$D_{m,i} = 0.54$

TABLE II
VFT PARAMETERS BASED ON 100 MVA RATING

Variable Frequency Transformer		Control system	
Parameter	Typical value	Parameter	Value
X_{VFT}	12%	Kpp	0.005
$X_{mag,VFT}$	5.6 pu	Kip	3.00
X_{Ts} and X_{Tr}	10%	Kpω	0.40
Shunt Compensation	20 %	Kiω	0.001
H_i	25 pu-sec	τ	0.01

VIII. ACKNOWLEDGMENT

L. Contreras-Aguilar wishes to thank the National Council of Science and Technology of México (CONACyT) for financial support to carry out Ph.D. studies at the Universidad Michoacana de San Nicolás de Hidalgo.

IX. REFERENCES

[1] R. J. Piwko et al. "Variable Frequency Transformer-A New Alternative For Asynchronous Power Transfer", *Proc. IEEE Power Engineering Society,* Durban Africa, pp. 393-398, 11-15 July, 2005.

[2] D. Mc Nabb et al. "Transient and Dynamic Modeling of the New Langlois VFT Asynchronous Tie and Validation with Commissioning Tests", *Proc. International Conference on Power Systems Transients* (IPST'05), Canada, pp. 1-6. June, 2005.

[3] G. Chen and X. Zhou, "Digital Simulation of Variable Frequency Transformers for Asynchronous Interconnection in Power System", *Proc. IEEE Power Engineering Society Transmission and Distribution Conf.*, Dalian China, pp. 1-6, Dec. 2005.

[4] P. Hassink et al. "Second & Future Applications of Stability Enhancement in ERCOT with Asynchronous Interconnections", *Proc. IEEE Power Engineering Society General Meeting*, Florida USA, pp. 1-7, June 2007.

[5] E. R. Pratico et al. "VFT Operational Over-view - The Laredo Project", *Proc. 2007 IEEE Power Engineering Society General Meeting*, Florida USA, pp. 1-6, July 2007.

[6] B. Bagen et al. "Evaluation of the Performance of Back-to-Back HVDC Converter and Variable Frequency Transformer for Power Flow Control in a Weak Interconnection", *Proc. IEEE Power Engineering Society General Meeting*, Florida USA, pp. 1-6, June 2007.

[7] J. Adams et al. "Planning for uncertainty: NYISO planning process and smart grid", *Proc. IEEE Power Engineering Society General Meeting*, págs. Pittsburgh USA, pp. 1-4, July 2008.

[8] P. C. Krause, O. Wasynczuk and S. D. Sudhoff, "*Analysis of Electric Machinery*", New York: McGraw Hill, 1987.

[9] T. S. Parker and L. O. Chua, "Practical Numerical Algorithms for Chaotic Systems", NY: Springer Verlag, 1989.

[10] A. Semlyen and A. Medina, "Computation of the Periodic Steady State in Systems with Nonlinear Components Using a Hybrid Time and Frequency Domain Methodology", *IEEE Trans. Power Systems*, Vol. 10, No. 3, pp. 1489-1504, Aug. 1995.

[11] K. Astrom and T. Hagglund, "PID Controllers: Theory, Desing and Tuning", Swedden: Instrument Society of America, 1995.

X. BIOGRAPHIES

L. Contreras-Aguilar received the mechanical-electrical engineering degree from the Universidad de Colima, Colima, México, in 2002. He got his M.Sc. degree from the Universidad Michoacana de San Nicolás de Hidalgo, México, in 2005. Currently, he is pursuing the Ph.D. degree in power systems at the UMSNH, Morelia, México.

N. García received the electrical engineering degree from the Universidad Michoacana de San Nicolás de Hidalgo, Morelia, México, in 1993 and the M.Sc. degree from the Universidad Michoacana, México, in 1999. He obtained his Ph.D. degree from the University of Glasgow, Glasgow, Scotland, U.K, in 2003. At present, he holds a permanent position as a research professor at the Facultad de Ingeniería Eléctrica, UMSNH, Morelia, México.